Communications Earth & Environment https://doi.org/10.1038/s43247-026-03408-z

Article in Press

Pre-subduction of the Caroline Plateau intensifies lithospheric hydration in the southern Mariana Trench

Received: 16 October 2025

Accepted: 6 March 2026

Cite this article as: He, E., Qiu, X., Li, Y. *et al.* Pre-subduction of the Caroline Plateau intensifies lithospheric hydration in the southern Mariana Trench. *Commun Earth Environ* (2026). https://doi.org/10.1038/s43247-026-03408-z

Enyuan He, Xuelin Qiu, Yuhan Li, Ingo Grevemeyer, Min Xu, Minghui Zhao, Yuan Wang, Chuanxu Chen & Jiangyang Zhang

Pre-subduction of the Caroline Plateau intensifies lithospheric hydration in the southern Mariana Trench

Enyuan He[1], Xuelin Qiu[1*], Yuhan Li[2], Ingo Grevemeyer[2], Min Xu[1], Minghui Zhao[1], Yuan Wang[3], Chuanxu Chen[4], Jiangyang Zhang[1]

[1]State Key Laboratory of Tropical Oceanography, South China Sea Institute of Oceanology, Chinese Academy of Sciences, Guangzhou 510301, China

[2]GEOMAR Helmholtz Centre for Ocean Research Kiel, Kiel 24148, Germany

[3] Key Laboratory of Deep Petroleum Intelligent Exploration and Development, Institute of Geology and Geophysics, Chinese Academy of Sciences, Beijing 100029, China

[4]Institute of Deep-Sea Science and Engineering, Chinese Academy of Sciences, Sanya 572000, China

Corresponding author: Xuelin Qiu (xlqiu@scsio.ac.cn)

ABSTRACT

The subduction of oceanic plateaus significantly reshapes subduction systems, yet its impact on lithospheric hydration prior to subduction is not well understood. Here we investigate these processes as the Caroline Plateau approaches the southern Mariana Trench, using velocity models derived from wide-angle seismic lines. Our results from OBS2017-1 reveal that the crust of the subducting plate thickens from ~7.5 km beneath the trench axis to ~16.0 km at the outer rise, accompanied by reduced seismic velocities in the region between the toe of the plateau and the trench axis. These velocity reductions even exceed those observed beneath adjacent oceanic crust near Challenger Deep, indicating intensified hydration at the leading edge of the plateau, further supported by a narrowing of the bending-related faulting zone. The simultaneous subduction of plateau and normal oceanic crust governs plate configuration, highlighting the role of oceanic plateaus in enhancing heterogeneous water percolation and modulating subduction dynamics.

Keywords: Southern Mariana Trench, Caroline Plateau, Lithospheric Hydration, P-wave Velocity Structure, Wide-angle Seismic Data

Introduction

Subduction zones are crucial pathways for transferring and recycling surface materials deep into the Earth's interior, nurturing interactions between multiple layers of the Earth system. These processes are fundamental to understanding the planet's habitability[1]. Hydration of the subducting plates significantly affects subduction

dynamics. As oceanic lithosphere bends before being subducted, it experiences tensional faulting and crustal fracturing that promote water-rock interactions and serpentinization of upper mantle rocks, introducing significant amounts of water into the subduction system[2,3]. This hydration process is the primary mechanism for transporting water into the deep Earth[4,5]. After entering subduction zones, subducted slabs can dehydrate at various depths, contributing to the formation of trench-arc-basin systems or the storage of water within the mantle[6]. The continuous cycle of hydration and dehydration drives tectonic deformation, magmatism, and seismicity, shaping Earth's most active seismic, volcanic, and mineral belts[7].

In addition to oceanic crust, subducting plates may also carry oceanic plateaus into the deep mantle[8]. Oceanic plateaus, which are manifestations of large igneous provinces (LIPs), are characterized by over-thickened crust (average thickness of 21±4 km) with high buoyancy[9]. Their subduction reshapes the tectonic configuration of subduction zones, influencing trench morphology and causing displacements in the trench-arc-basin system. Upon entering trenches, these buoyant plateaus may either accrete to the overriding plate or subduct beneath it at shallow angles[10]. This process results in trench migration or subduction zone reorientation, where the old subduction zone ceases and a new one initiates behind the plateau[9]. After oceanic plateaus enter subduction zones, the slab may experience displacement[11], tearing[12], or break-off[13]. Previous studies have primarily focused on the processes following the entry of plateaus into subduction systems, yet the pre-subduction effects of oceanic plateaus on bending and hydration remain poorly understood. Studying these effects is crucial for comprehending the entire subduction process, including geodynamic and compositional interactions between the subducted plateau and the deep mantle.

The Izu-Bonin-Mariana (IBM) Trench, spanning over 2,800 km between the Pacific and Philippine Sea plates, is a natural laboratory for studying intra-oceanic convergent margins[14]. This study focuses on the southern Mariana trench (Fig. 1a), home to the Challenger Deep, the Earth's deepest point, where the ~125 Ma Pacific Plate subducts with pronounced flexure[15,16]. The Caroline Plateau, which is a LIP formed by the Caroline mantle plume at <30 Ma[17], lies 60–120 km west of the Challenger Deep and appears to affect the southern Mariana subduction zone, impacting its topography, seismicity, and plate configuration[18–20]. However, the nature and extent of this impact remain unclear, highlighting the need for detailed imaging of the crust and upper mantle structure of the subducting plate.

In 2016–2017, the Chinese Academy of Sciences (CAS) conducted three research cruises at the southern Mariana Trench, acquiring four active-source ocean bottom seismometer (OBS) profiles perpendicular to the trench (Fig. 1a). Profiles OBS2016-1 and OBS2016-2 employed rated to 6,000 m and 9,000 m water depth, respectively. In 2017, the application of newly developed 10,000 m-rated OBSs enabled the acquisition of profiles OBS2017-1, and OBS2017-2 across the Challenger Deep. Data from OBS2016-1 imaged a 12.0–14.0

km thick subducting oceanic plateau[21], while OBS2016-2 revealed a highly serpentinized mantle beneath the normal oceanic crust (6.5–7.0 km thick) of the subducting Pacific plate[22]. The velocity structure along profile OBS2017-2 demonstrates the subducting plate has normal crustal thickness (6.5–7.2 km) but reduced velocities relative to mature Pacific crust[23]. Additionally, a low-velocity layer with high V_p/V_s ratios (1.80–1.95) was detected beneath the oceanic crust, suggesting a srtongly serpentinized layer with a rapid transition at its base[23,24]. The velocity structures of these three published OBS profiles reveal some lateral variability in crustal thickness and velocity reductions in the crust and upper mantle of the subducting plate, thereby highlighting the along-strike transition between the oceanic plateau and normal oceanic crust as they converge towards the trench.

Profile OBS2017-1 located in the middle between and oriented parallel to profiles OBS2017-2 and OBS2016-1 (Fig. 1a). This study focuses on its southern segment extending from the trench axis to the Caroline Plateau with 15 OBSs available. We use these data to elucidate the structural variations in the crust and upper mantle as the Caroline Plateau approaches the trench. The unique position of OBS2017-1 allows us to investigate such variations in two directions: along the profile itself, and along the trench axis with the help of other profiles. By integrating multibeam bathymetry, seismic activity, and gravity anomaly data, we reveal how the juxtaposition of the oceanic plateau and normal oceanic crust on the subducting plate affects the subduction system. Our findings enhance understanding the effects of an incoming oceanic plateau on hydration processes and heterogeneous water percolation.

Results and discussion

The final velocity structure along OBS2017-1 exhibits significant variations towards the trench (Figs. 2a–c), with the Moho depth deepening beneath the plateau and crustal thickness of the subducting plate ranging from 7.5 km to 18.0 km. Seismic record sections (e.g., Fig. 2d) show the high quality of our dataset. Based on velocity structure and seafloor topography, the model is divided into two segments: the bending-related faulting zone (model distance 0–80 km) and the Caroline Plateau region (model distance 80–150 km). The faulting zone is further subdivided into the outer trench slope (model distance 0–35 km) and the outer rise (model distance 35–80 km), characterized by progressive changes in crustal thickness and fault intensity.

Faulting and hydration processes in the simultaneous subduction of oceanic plateau and normal oceanic crust

The outer trench slope (model distance 0–35 km) has a crustal thickness of 7.5–9.0 km (Fig. 2a), which is thicker than mature Pacific oceanic crust (5.3–7.0 km)[25,26], yet exhibits notably lower crustal velocities. Upper mantle velocities in this region range from 7.0 to 7.2 km/s, significantly below the typical dry mantle velocity of 8.0 km/s[26]. In the outer rise region, the crust thickens further to 9.0–12.0 km, intermediate between normal

oceanic crust and the thicker Caroline Plateau. In the Caroline Plateau region (model distance 80–150 km), crustal thickness reaches 16.0–18.0 km. One-dimensional velocity-depth profiles in this segment fall outside the ranges of both typical oceanic and continental crust but closely resemble global oceanic plateau structure[27], indicating an oceanic plateau composition for the Caroline Plateau (Fig. 3a). High-resolution bathymetry reveals abundant trench-parallel normal faults in the outer trench slope and outer rise[28], accompanied by significant seismicity at depths of 10–50 km[20,29] and evidence of fluid discharge at the seafloor[30]. These characteristics align with findings from other subduction zones[31–33], suggesting that bending-related faulting and hydration play a critical role in modifying the subducting plate.

Notably, the onset of bending-related faulting observed in bathymetric data does not coincide with the location of significant P-wave velocity (V_p) reduction (Fig. 2a). Faults initiate at ~80 km from the trench (Fig. 2b), where the crust is 14.0–16.0 km thick, yet no substantial decrease in crustal or upper mantle velocities is observed (Fig. 2c). This indicates that initial faulting has limited impact on crustal alteration or hydration in this zone. At ~45 km from the trench, where the crust thins to ~10.0 km, the 7.0 km/s iso-velocity contour drops rapidly, and upper mantle V_p decreases to 7.4 km/s. This velocity is significantly lower than that in the fault initiation zone (45–80 km from the trench, upper mantle V_p ~7.8 km/s) and the typical dry mantle value (8.0 km/s), indicating that faults have penetrated through the entire crust and reached the uppermost mantle, initiating serpentinization. On the outer trench slope, the 6.5 km/s velocity contour drops rapidly to the base of the crust, and upper mantle velocities further decrease to 7.0–7.2 km/s (Figs. 2a–c). This area also shows a sharp increase in water depth and a higher density of closely spaced normal faults (Fig. 2b), indicating intensified bending-related faulting and extensive mantle hydration.

Based on these observations along profile OBS2017-1, we propose a three-stage model of progressive bending-related faulting and hydration towards the trench: (1) Stage 1 (80–45 km): Initiation of normal faulting in the shallow crust, resulting in seafloor fault offsets but no significant velocity reduction. (2) Stage 2 (45–35 km): Faults propagate into the thinned crust and reach the uppermost mantle, initiating limited serpentinization. (3) Stage 3 (35–0 km): Pervasive faulting throughout the crust and into the deeper mantle, leading to intensive serpentinization. The spatial mismatch between the initiation of faulting and velocity reduction reflects the progressive deepening of faults and increasing hydration with proximity to the trench.

The approach of the oceanic plateau towards the trench enhances crustal fragmentation and mantle serpentinization between the leading edge of the plateau and the trench. At equivalent distances (20 km) from the trench, crustal and upper mantle velocities along profile OBS2017-1 are lower than those along OBS2017-2 and OBS2016-2 (Fig. 3b), indicating stronger faulting and serpentinization. Furthermore, velocities near the trench are lower than in subduction zones such as Chile and Nicaragua (Fig. 3c) and generally lower than in

most global subduction zones[25]. We can exclude the possibility that the velocity reduction along OBS2017-1 is inherited from low velocities at the transition from the oceanic crust to the oceanic plateau because no such observation was found in global oceanic plateaus, such as the Kerguelen Plateau[34] and the Louisville Ridge[35]. Bathymetric data reveal systematic east-to-west narrowing in the extent of faulting. Along profile OBS2017-1, the initial faulting begins at 80 km from the trench; to the east, in the Challenger Deep region, it starts at 110–120 km (Figs. 1a and 1c). Similarly, the zone of extremely low upper mantle velocities (<7.5 km/s) extends only ~45 km from the trench along OBS2017-1, whereas it reaches 90–110 km along OBS2017-2 and OBS2016-2 in the Challenger Deep region (Fig. 4). Plate curvature is also more pronounced in the plateau region (OBS2017-1) than in the Challenger Deep (Fig. 1c). These patterns suggest that the approaching oceanic plateau localizes bending deformation at its leading edge, enhancing fracturing and hydration. Numerical simulations by Zhang et al.[36] show that when a high-rigidity plateau approaches the trench, bending deformation concentrates at its front, which is consistent with our observations. Similar velocity patterns have been reported during the subduction of the Roo Rise plateau at the Java Trench[37]. Even smaller features like seamounts, though less extensive, can promote enhanced fracturing and serpentinization in leading crust[38].

Upon entering the trench, the oceanic plateau exhibits distinct faulting behavior and hydration characteristics compared to the adjacent oceanic crust. In the oceanic crustal domain, normal faults are denser but have smaller throws (<750 m). In contrast, in the plateau domain, faults are sparser but exhibit larger throws (750–1250 m) (Fig. 4a and Supplementary Fig. S20). This structural contrast observed from bathymetry corresponds to the variation in velocity reductions. Upper mantle velocities beneath the outer trench slope increase progressively from ~7.0–7.2 km/s along profiles OBS2017-1 and OBS2017-2[22,23] to 7.4–7.5 km/s beneath profile OBS2016-1[21] (Figs. 4b–4e), indicating progressively reduced serpentinization from the oceanic crust to the plateau domain. Boneh et al.[39] proposed that the extent of mantle serpentinization depends on the combined effect of fault throw and fault density, which together increase the volume of damage zone prior to subduction. The cumulative fault throws within 30 km of the trench are 5766 m and 4233 m along profiles OBS2017-1 and OBS2017-2, respectively, which are both exceeding that along profile OBS2016-1 (2912 m) (Supplementary Fig. S20). Accordingly, the more intensive faulting in the oceanic crustal domain likely promotes greater mantle hydration than in the plateau domain. This interpretation is consistent with seismicity patterns within the subducted slab. Chen et al.[40] reported along-strike variations in intermediate-depth earthquakes: a double seismic zone in the Pacific segment and a single zone in the Caroline Plateau segment, which are attributed to limited hydration due to the plateau's thickened crust. The velocity structures across these domains (Figs. 4b–4e) support the earthquake observations, suggesting that contrasting crustal structures exert a first-order control on pre-subduction faulting, hydration, and post-subduction dehydration processes.

Du et al.[30] highlight that fluid discharge points near normal faults (Figs. 1a) are associated with basaltic crust alteration. Specifically, discharge sites P and M are located near OBS30 and OBS31 (Fig. 2b), coinciding with regions of sharp velocity reduction in the crust and upper mantle (Fig. 2c). This suggests that bending-related faults act as major conduits for fluid migration and water-rock interactions. Assuming a correlation between fault characteristics, velocity reduction, and hydration intensity, we infer that such interactions peak at OBS2017-1, slightly decrease towards the Challenger Deep (OBS2017-2), and weaken markedly further west (OBS2016-1).

Geophysical surveys and numerical modeling studies show that oceanic plateaus can cause slab displacement[11], tearing[12], or break off[13] when entering subduction zones, potentially triggering trench migration, where the old subduction zone ceases and a new one initiates behind the plateau. Our findings reveal intensified and localized crustal fracturing and mantle serpentinization at the leading edge of the incoming plateau. These weakened zones, once subducted, are more prone to rupture, dehydration, and melting, increasing the likelihood of slab tearing, fragmentation, and detachment.

Effects of the simultaneous subduction of oceanic plateau and normal oceanic crust on the incoming and overriding plates

The main body of the Caroline Plateau can be clearly outlined by the 3000-m isobath and is confirmed to subduct west of 140°30′E. However, the bathymetry alone does not fully resolve the complete extent of the Caroline Plateau. Crustal structure variations along the southern Mariana Trench reveal a gradual transition from typical oceanic crust (6.5–7.2 km thick) near the Challenger Deep (profiles OBS2016-2 and OBS2017-2) to the thicker Caroline Plateau (12.0–14.0 km) along profile OBS2016-1 (Fig. 4). The velocity structure along OBS2017-1 further captures the margin of the oceanic plateau. While evident in seismic profiles, the lateral extent of this marginal zone remains uncertain due to sparse trench-perpendicular profiles and the lack of trench-parallel observations.

To better constrain this boundary, we use Bouguer gravity anomalies, which reflect lateral variations in crustal and upper mantle density. High Bouguer anomalies correlate with thinner crust or cooler mantle, while low anomalies indicate thicker crust or hotter mantle[41]. Along the western side of profile OBS2017-1, low anomalies (400 to 500 mGal) correspond to crustal thickness of 12.0–18.0 km, as revealed by OBS data (Fig. 5c). On the eastern side, higher anomalies (>500 mGal) correspond to a thinner crust of ~7.0 km. Integrating crustal thickness and gravity data allows us to delineate the boundary between the oceanic plateau and normal oceanic crust (Fig. 5c). The improved delineation of the plateau's extent based on four OBS profiles, which

reveal that its geophysical defined boundary extends outward beyond the 3000-m isobath into deeper water depths.

Different subducting segments correspond to distinct tectonic responses in the overriding plate (Fig. 5). Where the oceanic plateau subducts, the inner trench slope uplifts, forming an arch-like topography. In contrast, where normal oceanic crust subducts, the inner trench slope widens and the arch disappears (Figs. 5a and 5d). This suggests that the buoyant, elevated plateau exerts compressive forces, whereas subduction of less buoyant oceanic crust results in weaker compression. Miura et al.[42] reported that the upper part of the Ontong Java Plateau underwent collision-related accretion to the landward side, leading to a velocity increase of ~0.2 km/s and crustal thickening of ~5 km within the 80-km-wide Malaita Accretionary Prism, and the absence of a discernible top interface of subducted plateau. However, a similar velocity structure in the uplifted inner trench along profile OBS2016-1 in our study area can be estimated as a <4 km thick and 20 km wide accretionary prism[21], contrasting with the features of accretionary prisms near the Ontong Java Plateau. This comparison, together with the clearly identifiable top interface of the subducted Caroline Plateau[21], suggests that the Caroline Plateau has experienced subduction rather than collision-related accretion. Landward, within the back-arc region, the plateau segment shows no rift topography and only sparse thrust and strike-slip earthquakes (Figs. 5a and 5d). In contrast, the oceanic crust segment features the incipient Southwest Mariana Rift (SWMR), marked by trench-parallel extensional faults[43], lineament fabrics[44], and seismicity[20,45]. Further east, the region transitions into the Diffuse Spreading Zone (DSZ), characterized by high Bouguer anomalies and both trench-parallel and trench-perpendicular extensional earthquakes[46].

Back-arc spreading dynamics is affected by both the subducted slab and the overriding plate[47]. The Philippine Sea Plate is drifting towards the Eurasian continent at a rate of 23–136 mm/a in a WNW direction[48]. However, this far-field motion alone cannot explain the rapid stress transition observed over such short distances in the back-arc region. Seismicity data indicate that the length of subducted slab increases gradually from ~100 km at the oceanic plateau segment to ~140–160 km near the Challenger Deep and ~240 km near Guam[20]. The average dip angle of the subducted slab also increases from ~30° to ~60° at depths >30 km[20]. The morphology of the subducted slab correlates strongly with the topography and stress distribution in the back-arc region of the overriding plate (Fig. 4a), as well as with variations in faulting and serpentinization within the incoming plate prior to subduction (Fig. 3). Three-dimensional tomographic images derived from local earthquake travel-time data reveal an increasing dip angle of the subducted Pacific slab with depth near the Challenger Deep, suggesting rapid slab rollback[49]. This eastward increase in rollback degree may be the primary driver of the rapid tectonic changes in the back-arc region. We speculate that the more buoyant oceanic plateau resists subduction, leading

to a shorter subducted slab in the plateau region compared to the oceanic crust domain. In contrast, the longer slab at the oceanic crust segment is more susceptible to gravitational rollback, further increasing its dip angle.

The Hikurangi subduction zone also shows along-trench thinning of the incoming crust from ~11 ± 1 km in the south to ~7 ± 1 km in the north[50–52], affecting subducting plate geometry and the stress state of overriding plate[51]. In comparison, the crust of Caroline Plateau is thicker (12–14 km) and shows more rapid thinning in the trench-parallel direction, driving the more pronounced segmentation of the overriding plate described above.

As conclusions, we compile three scenarios of plateau–subduction interaction along the southern Mariana Trench, based on three trench-perpendicular OBS profiles: (a) Plateau far from the trench. The Pacific lithosphere undergoes broad flexure, characterized by dense arrays of small-offset faults and widespread velocity reductions, indicative of strong fracturing and hydration (Fig. 6a). (b) Plateau approaching the trench. Contrasting rigidity between the plateau and adjacent crust localizes bending and faulting to the region between the plateau toe and the trench axis, while the plateau itself is less deformed. The deformation zone narrows (~80 km), and velocity reductions are confined (~45 km) but with stronger serpentinization than in the Challenger Deep (Fig. 6b). (c) Plateau with a thickness of ~12 km entering the trench. The plateau itself begins to fracture, but its high strength and thick crust result in sparse, large-offset faults and only modest velocity reductions, implying weaker hydration than in normal oceanic crust (Fig. 6c). The buoyant plateau induces compressional and strike-slip stresses in the overriding plate, causing inner trench slope arching and suppressing back-arc rifting. In contrast, subduction of normal oceanic crust promotes extensional stress, absence of arching, and incipient back-arc rifting driven by slab rollback. These scenarios not only reflect the current spatial relationship between the Caroline plateau and the Mariana Trench but also hold temporal implications. With the continuous subduction of the Pacific Plate, the plateau far from the trench (Fig. 6a) will gradually transition to approaching (Fig. 6b), then to entering the trench (Fig. 6c). Eventually, the subduction of Caroline Plateau will occur at the Challenger Deep, further highlighting the dynamic evolution of plateau-subduction interactions.

Methods

Data acquisition. The 430 km-long wide-angle seismic refraction profile OBS2017-1 was acquired perpendicular to the southern Mariana Trench (Fig. 1a). A total of 40 OBSs were deployed at 10 km intervals along the profile, with 38 successfully recovered but 2 lost. This study focuses on a 170 km segment of the subducting Pacific Plate, running from the Caroline Plateau to the trench axis, encompassing the bending fault zone. In order to optimally constrain the velocity structure of the subducting plate, 15 OBS stations that recorded the best data quality in this dataset were selected for analysis. The stations located on the overriding plate were

not employed in this work because the low signal-to-noise ratio of the refractions turning from the subducting plate and the unconstrained geometry of the subducting slab prevent a robust control on the velocity structure here using these stations. These selected stations include three 10,000 m-rated instruments (OBS26, OBS27, and OBS28), which were deployed in water depths exceeding 8,000 m and successfully recovered. The seismic source consisted of a four-air-gun array with a total volume of 6,000 in^3, fired at 80 s intervals with an average ship-speed of 5 knots, resulting in a total of 805 shots.

Seismic tomography. Processed seismic records provided high-quality data, enabling clear identification of refracted P-wave phases and wide-angle reflections from crustal interfaces (Supplementary Figs. S1–S15 and Text S1). The two-dimensional P-wave velocity (V_p) structure and the geometry of the seismic Moho discontinuity along profile OBS2017-1 were determined using the seismic tomography software TOMO2D[53], through a joint travel-time inversion of first-arrival refractions and secondary-arrival wide-angle reflections.

For constructing the starting model, the seafloor depth was extracted from high-resolution bathymetric data downloaded from the NOAA National Centers for Environmental Information (NCEI), the sedimentary velocity and basement were constrained by using RayInvr software[54] to forward the PbP and near-offset Pg arrivals (Supplementary Fig. S16). A 0.2–0.5 km thick sedimentary layer is set up and fixed during the inversion. The initial crustal velocities were given by the 1-D velocity of normal Pacific crust, which are hanged below the basement. The initial Moho depth was set at 20 km.

The inversion was performed using a layer-stripping approach, reconstructing the velocity structure from shallow to deep in three stages, each with 10 iterations and different seismic phases. Detailed modeling parameters are provided in Supplementary Table S1. The inversion converged to a final normalized chi-squared value close to 1, with a root-mean-square (RMS) travel-time residual of 89.1 ms, indicating a good fit to the observed data.

To evaluate model resolution and uncertainties, we conducted the derivative weight sum (DWS) analysis, checkboard resolution tests, and Monte Carlo uncertainty assessments (Supplementary Text S2 and Figs. S17–S19). The resulting model shows robust resolution in the outer trench slope and oceanic plateau regions, due to dense ray path coverage. Velocity uncertainties are generally less than 0.1 km/s within the crust, increasing to greater than 0.15 km/s near the model edges and at depths exceeding 22 km, where ray coverage is sparse. Moho depth uncertainties range from ±0.1 km to ±0.5 km between model distance of 10 km and 125 km, reaching a maximum of ±2.0 km at a model distance of -10 km (Supplementary Fig. S18b).

Quantitive assessment of faulting behavior. Quantification of bending-related faults is performed using Global Mapper software (version 17.0) to extract plan-view bathymetric images and cross-sectional seafloor topography. Fault throws on the outer trench slope are measured using the "3D Path Profile /Line of Sight Tool" function in Global Mapper.

Data availability

Raw OBS data can be found here: https://doi.org/10.57760/sciencedb.27212.

Code availability

Travel-time tomography was performed using the TOMO2D software[53], available at https://github.com/jun-korenaga/tomo2d.

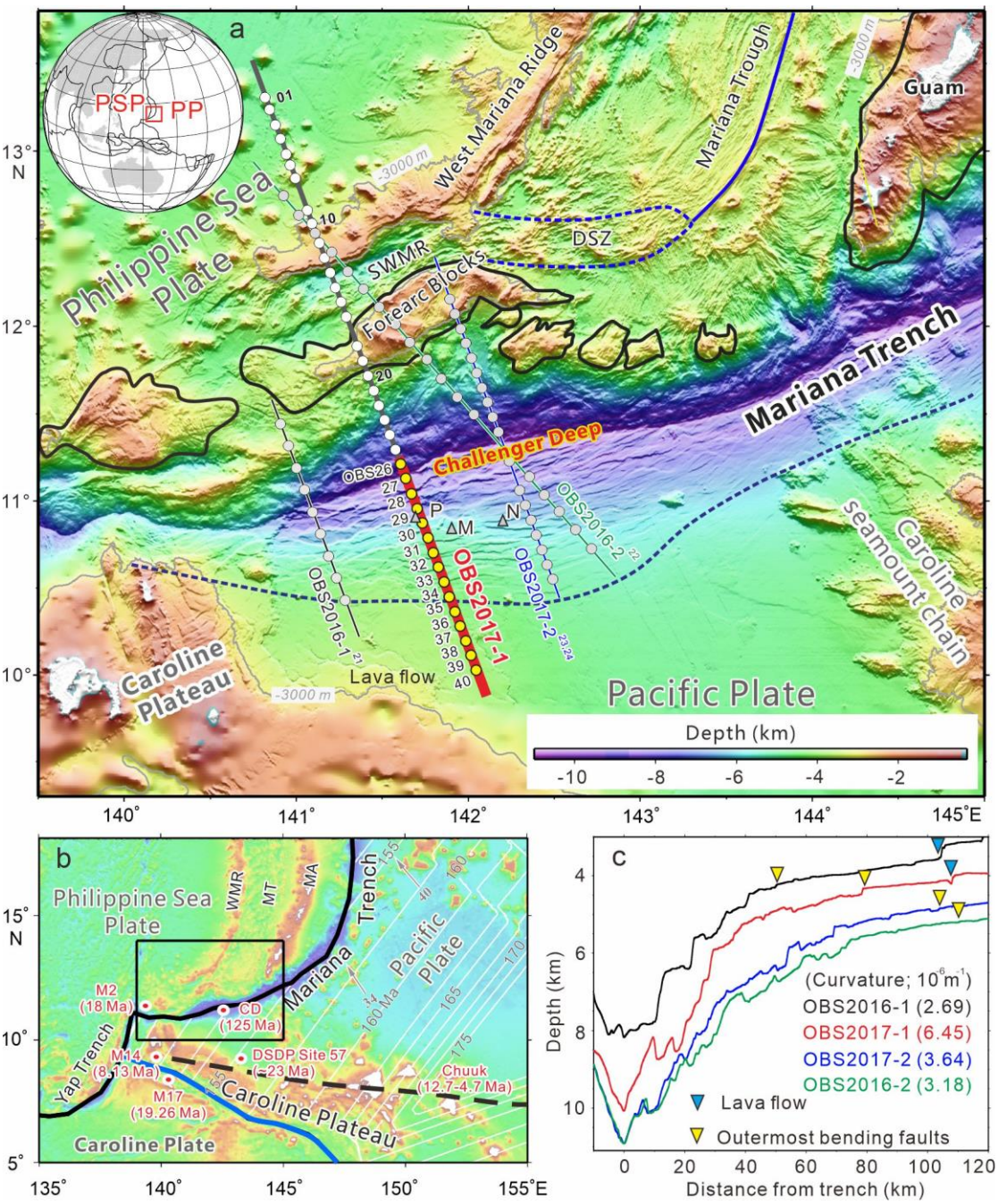

Fig. 1 | Tectonic setting of the southern Mariana subduction zone and OBS deployment. (a) Bathymetric map showing the location of the profile OBS2017-1 (thick red line) and OBS stations (solid yellow circles). The thin colorful lines and gray circles indicate previously published seismic profiles[21–24]. The black and blue curves on the overriding plate mark the forearc blocks and back-arc spreading centers (Mariana Trough and Diffuse Spreading Zone), respectively, modified from Martinez et al.[46]. The dashed dark blue line on the subducting plate indicates the onset of bending-related normal faults. The sites M, N, P (gray triangles) represent detected fluid discharge sites[30]. (b) Regional tectonic map showing the trajectory of the Caroline hotspot since 25 Ma[17,19]. The solid black line marks the trench, and the solid blue line delineates the boundary between the Caroline Plate and the Pacific

Plate[55]. Red circles denote dredging or drilling sites, with ages indicated in the brackets[17,56,57]. White lines are seafloor isochrons at 2.5 Ma intervals[58]. Convergence rate in mm/a and direction are from Bird[59]. (c) Detailed cross-sectional view of seafloor topography along multiple OBS profiles, highlighting variations in outer trench slope shapes and horst-and-graben structures caused by plate bending. Numbers in different colors within the parentheses denote the maximum curvature values on outer trench slope, using the same calculation method of Contreras-Reyes[60]. SWMR: Southwest Mariana Rift; DSZ: Diffuse Spreading Zone; PSP: Philippine Sea Plate; PP: Pacific Plate.

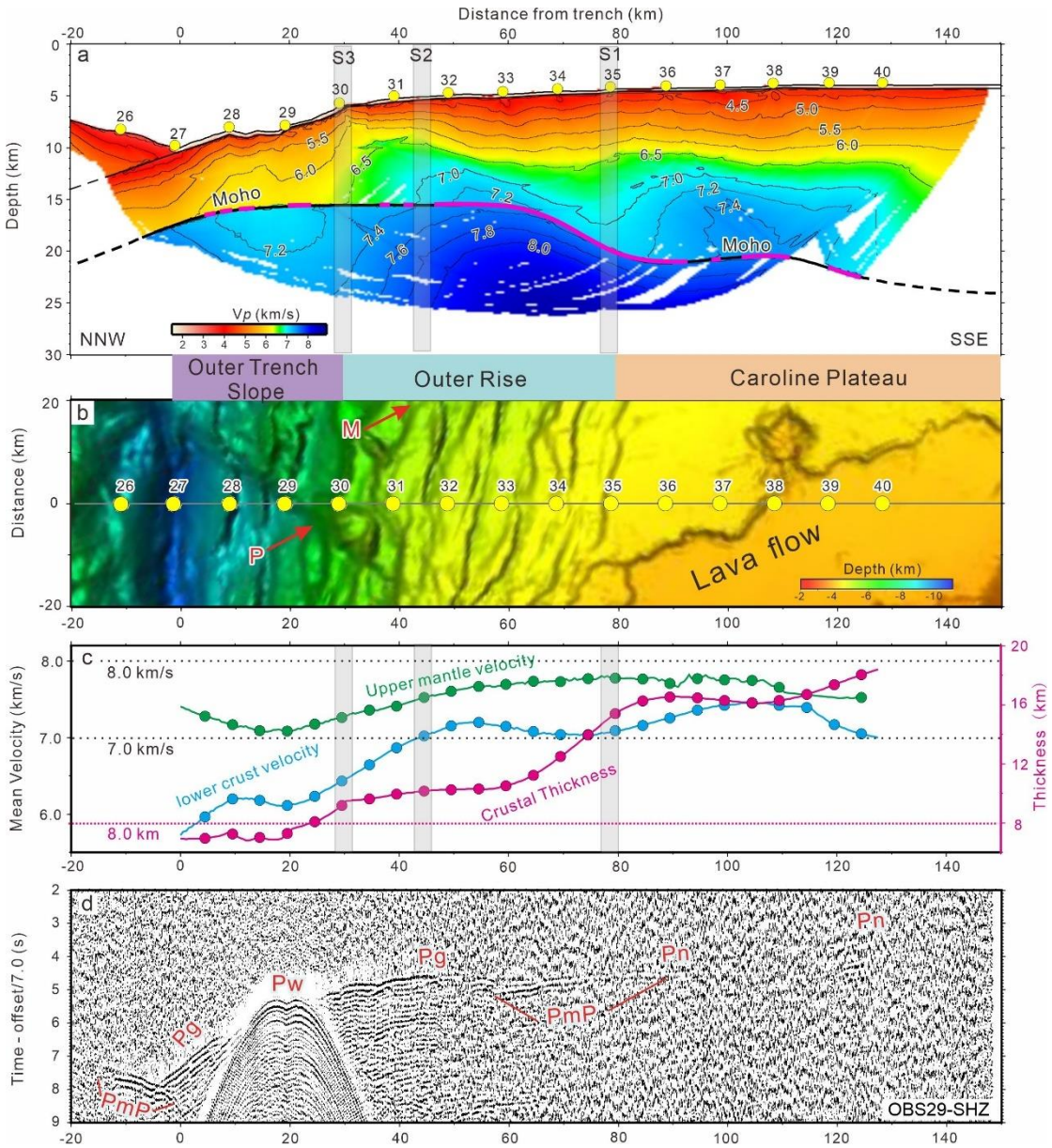

Fig. 2 | P-wave velocity tomographic model along profile OBS2017-1 (thick red line in Fig. 1a) and supporting data. (a) V_p model. Yellow dots on the seafloor show the locations of OBS. Pink solid lines indicate the Moho depth relatively well constrained by PmP arrivals. (b) Bathymetric map along the seismic line. Red arrows mark the fluid discharge sites[30]. Sites M and P mark the fluid discharge sites shown in Fig.1a. (c) Crustal thickness (pink line), and average velocity of lower crust (blue line) and upper mantle (green line) sampling from within 2 km above and below the Moho, respectively. (d) An example of wide-angle seismic record section of OBS 29 with identified seismic phases, also shown in Supplementary Figs. S4a and S4b.

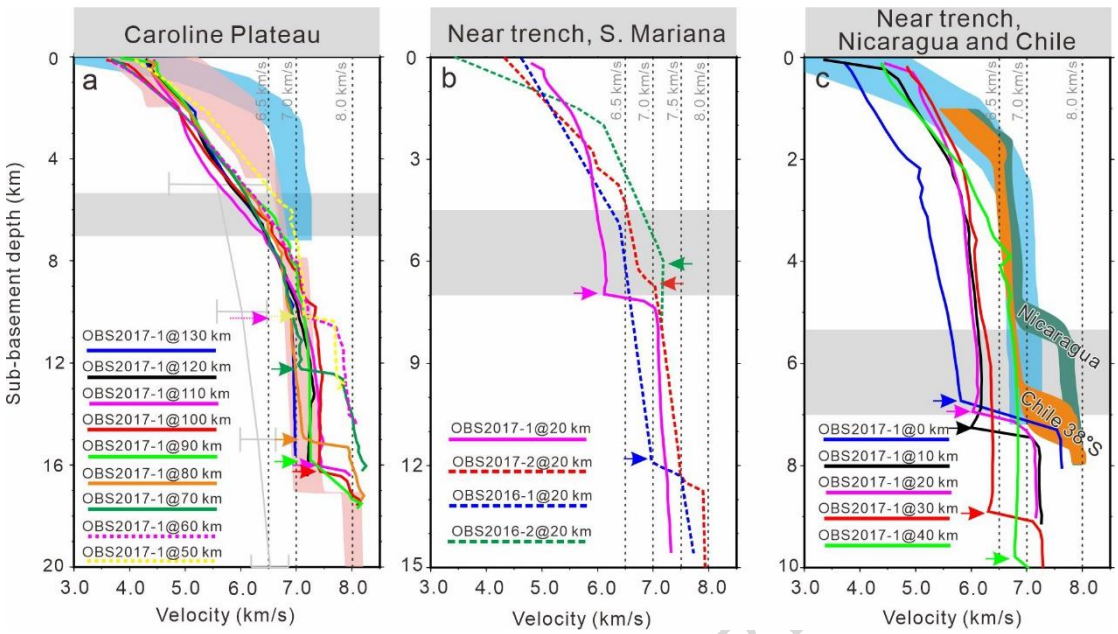

Fig. 3 | Comparison of 1D velocity-depth profiles extracted from OBS2017-1 model. The sampling locations of the 1D profile, spanning 0–130 km from the trench, correspond approximately one-to-one with OBS27 through OBS40. (a) Caroline Plateau with those of average continental crust (gray error bars)[61], mature Pacific oceanic crust (light blue envelope)[25], and compilation of oceanic Plateau crusts (light red envelope)[27]. OBS2017-1@130 km indicates the 1D profile sampled at 130 km from trench axis along profile OBS2017-1. Note that global oceanic plateau velocity-depth profiles are proportionally corrected to 17 km crustal thickness. The gray box denotes the thickness of Pacific oceanic crust[25]. Arrows show the Moho depth below basement with our own interpretations. (b) Near trench at 20 km along the southern Mariana trench. (c) Near trench with those from offshore Nicaragua (green envelope)[31] and Chile at 38°S (orange envelope)[32].

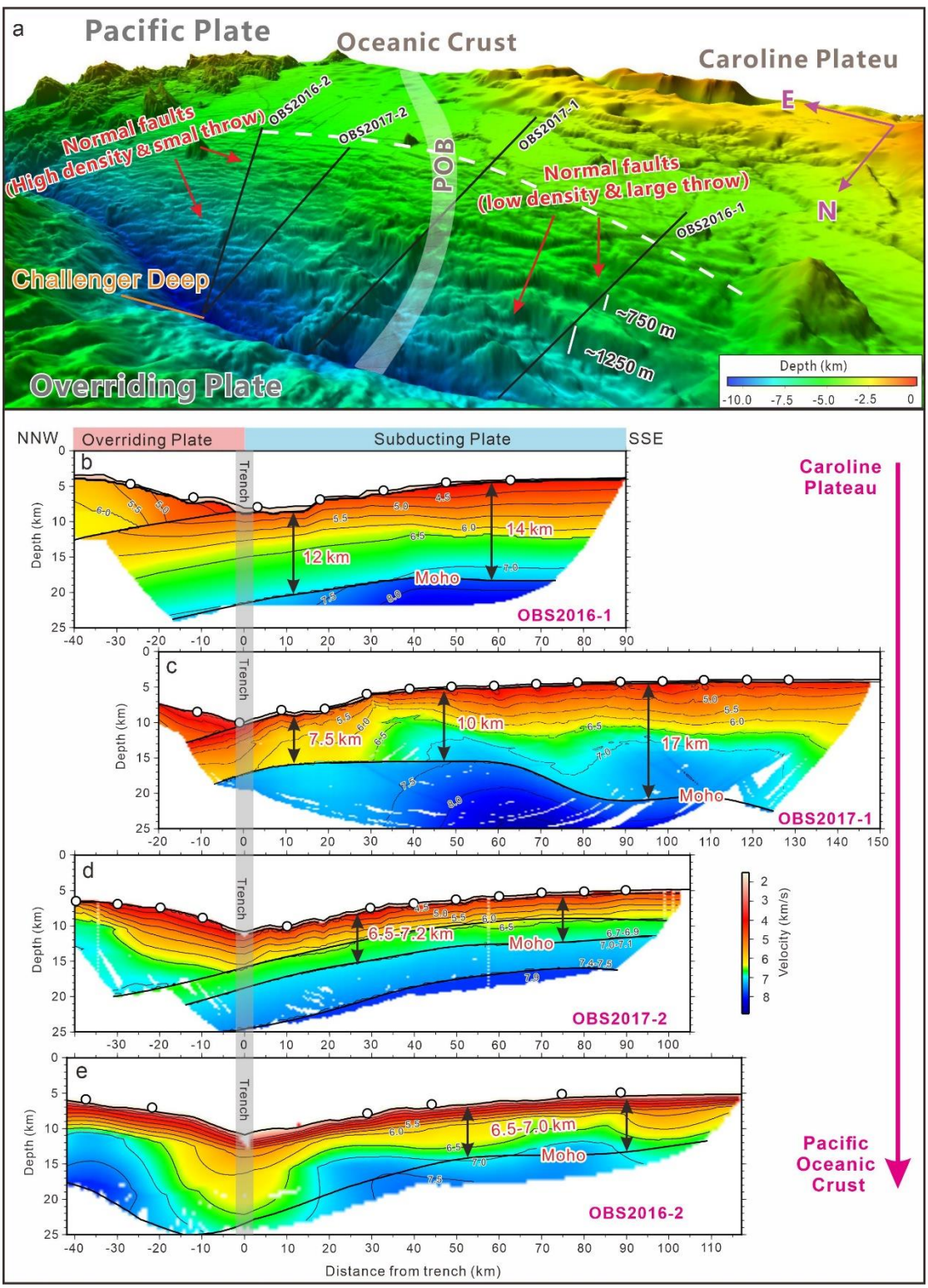

Fig. 4 | Trench-parallel variations in bending fault characteristics and V_p structure of the subducting plate. (a) Multibeam bathymetric map illustrating the change in normal fault behavior from the low-density and large-thrust at the oceanic plateau region to the high-density and small-thrust at normal oceanic crust (near the

Challenger Deep). (b-e) V_p structures along the four OBS profiles showing a gradual thinning in the crustal thickness from 12-14 km to 6.5-7.2 km. POB: Plateau and oceanic crust boundary.

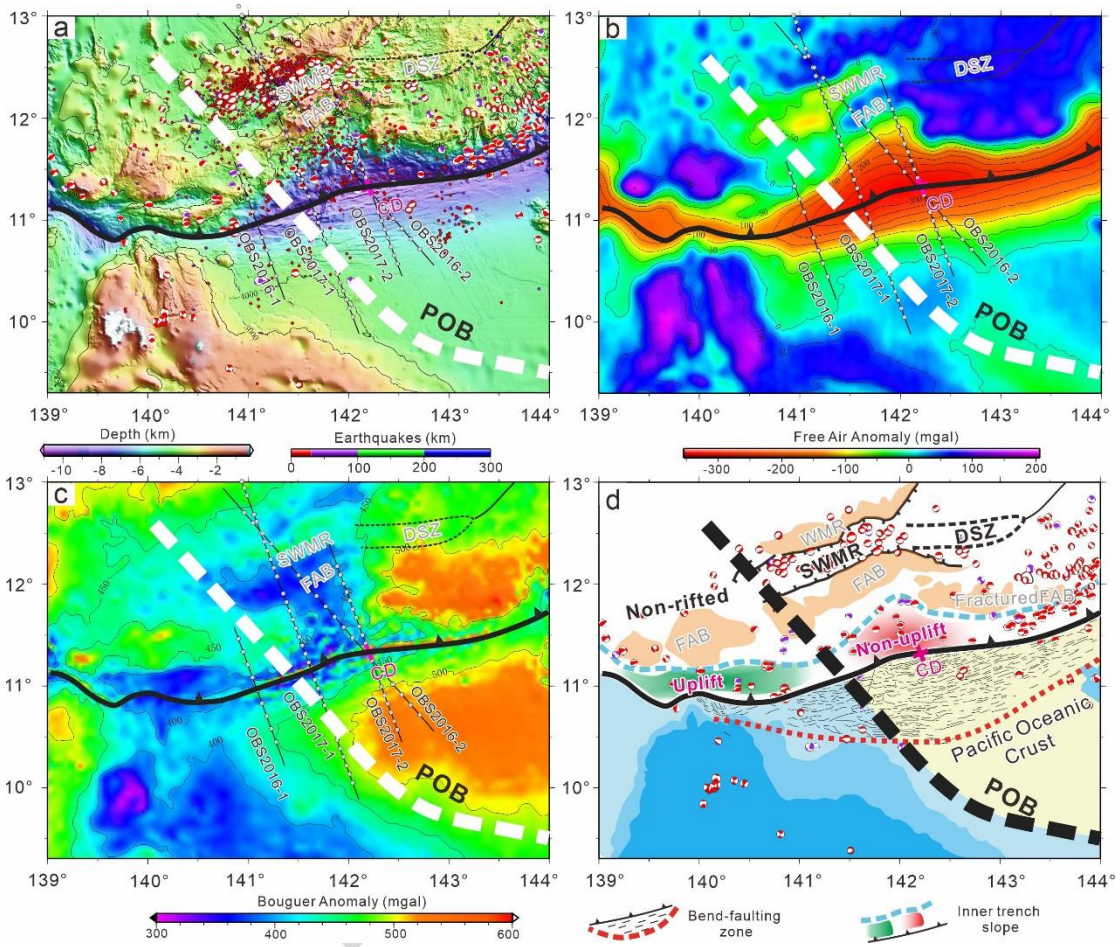

Fig. 5 | Seismicity, gravity anomalies, and tectonic interpretation. (a) Map of earthquake locations colored by depth. Solid circles are from Zhu et al.[20]. Earthquake focal mechanisms are from the Global Centroid Moment Tensor project [62]. (b) Satellite-derived free air gravity anomaly[63]. (c) Bouguer gravity anomaly. (d) Schematic illustration showing the relationship between the tectonic units of the subducting and overriding plates. POB: Plateau and Oceanic Crust Boundary; FAB: Forearc Blocks; SWMR: Southwest Mariana Rift; WMR: West Mariana Ridge; DSZ: Diffuse Spreading Zone; CD: Challenger Deep.

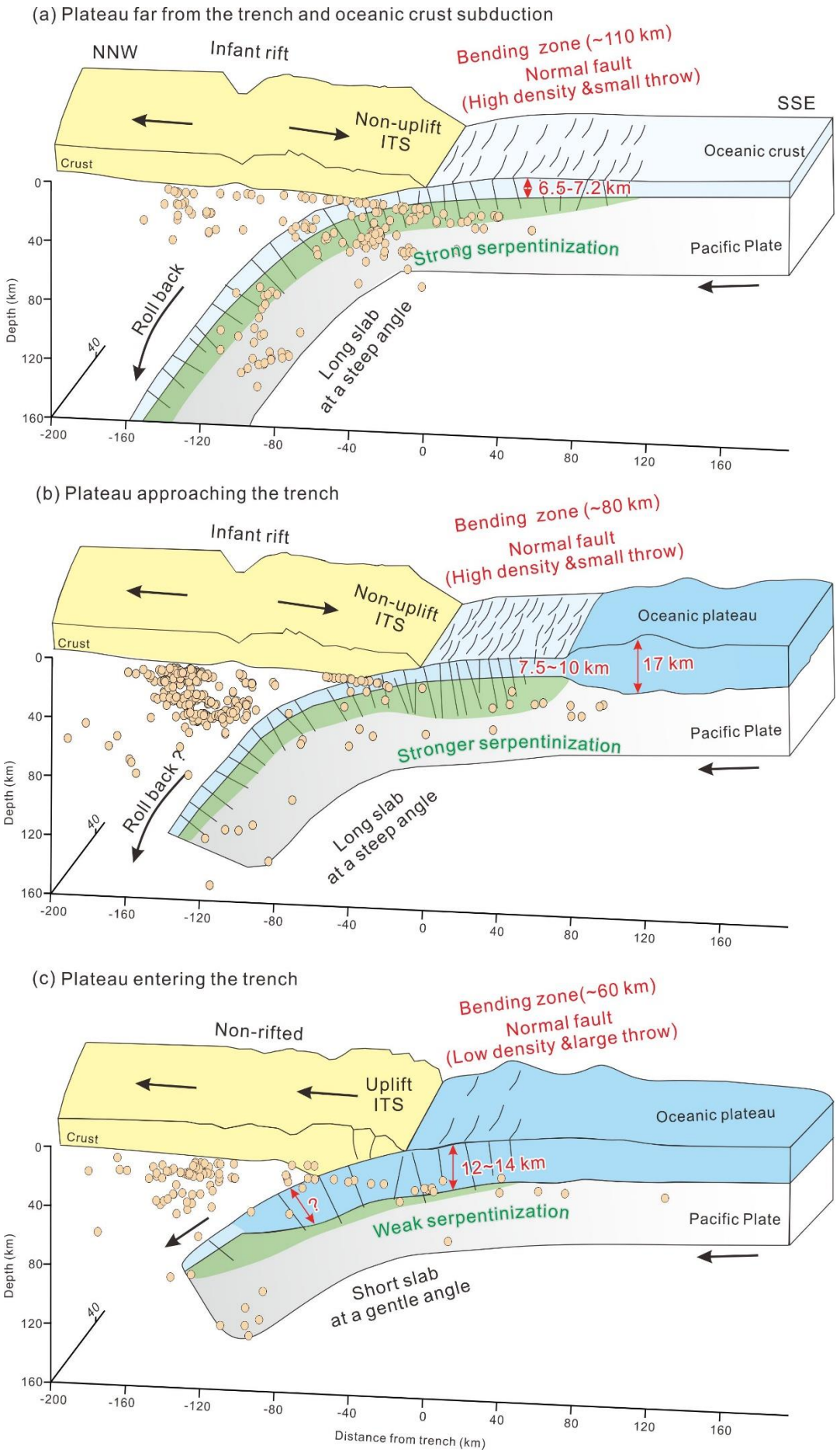
(a) Plateau far from the trench and oceanic crust subduction
NNW
Infant rift
Bending zone (~110 km)
Normal fault
(High density &small throw)
SSE
Non-uplift
ITS
Crust
Oceanic crust
6.5-7.2 km
Strong serpentinization
Pacific Plate
Roll back
Long slab
at a steep angle
Depth (km)
(b) Plateau approaching the trench
Infant rift
Bending zone (~80 km)
Normal fault
(High density &small throw)
Non-uplift
ITS
Crust
Oceanic plateau
7.5~10 km
17 km
Pacific Plate
Stronger serpentinization
Roll back ?
Long slab
at a steep angle
Depth (km)
(c) Plateau entering the trench
Non-rifted
Bending zone(~60 km)
Normal fault
(Low density &large throw)
Uplift
ITS
Crust
Oceanic plateau
12~14 km
?
Weak serpentinization
Pacific Plate
Short slab
at a gentle angle
Depth (km)
Distance from trench (km)

Fig. 6 | Interpretative cross-sections illustrating the plate bending and lithospheric hydration as an oceanic plateau approaches and enters the trench. These reconstructions are based on velocity models along three trench-perpendicular OBS profiles and regional geophysical data, incorporating seafloor topography, slab geometry, and earthquake distributions[20,40]. Three scenarios are shown: (a) when the plateau is far from the trench, (b) as it approaches, and (c) as it begins to subduct. ITS: Inner trench slope.

References

1. Xu, Y.-G. *et al.* Earth's habitability driven by deep processes (in chinese). *Chin. Sci. Bull.* **69**, 169–183 (2024).
2. Ranero, C. R., Phipps Morgan, J., McIntosh, K. & Reichert, C. Bending-related faulting and mantle serpentinization at the Middle America trench. *Nature* **425**, 367–373 (2003).
3. Cai, C., Wiens, D. A., Shen, W. & Eimer, M. Water input into the Mariana subduction zone estimated from ocean-bottom seismic data. *Nature* **563**, 389–392 (2018).
4. Rupke, L. Serpentine and the subduction zone water cycle. *Earth Planet. Sci. Lett.* **223**, 17–34 (2004).
5. Zhang, F. *et al.* Dual hydration of oceanic lithosphere. *Natl Sci Rev* **10**, nwad251 (2023).
6. Worzewski, T., Jegen, M., Kopp, H., Brasse, H. & Taylor Castillo, W. Magnetotelluric image of the fluid cycle in the Costa Rican subduction zone. *Nat. Geosci.* **4**, 108–111 (2011).
7. Li, J. *et al.* Dynamic processes of the curved subduction system in Southeast Asia: A review and future perspective. *Earth-Sci Rev* **217**, 103647 (2021).
8. Wei, S. S., Shearer, P. M., Lithgow-Bertelloni, C., Stixrude, L. & Tian, D. Oceanic plateau of the Hawaiian mantle plume head subducted to the uppermost lower mantle. *Science* **370**, 983–987.
9. Tetreault, J. L. & Buiter, S. J. H. Future accreted terranes: a compilation of island arcs, oceanic plateaus, submarine ridges, seamounts, and continental fragments. *Solid Earth* **5**, 1243–1275 (2014).
10. Gutscher, M., Spakman, W., Bijwaard, H. & Engdahl, E. R. Geodynamics of flat subduction: Seismicity and tomographic constraints from the Andean margin. *Tectonics* **19**, 814–833 (2000).
11. Arai, R. *et al.* Subduction of thick oceanic plateau and high-angle normal-fault earthquakes intersecting the slab. *Geophys. Res. Lett.* **44**, 6109–6115 (2017).
12. Menant, A., Sternai, P., Jolivet, L., Guillou-Frottier, L. & Gerya, T. 3D numerical modeling of mantle flow, crustal dynamics and magma genesis associated with slab roll-back and tearing: The eastern Mediterranean case. *Earth Planet. Sci. Lett.* **442**, 93–107 (2016).
13. Arrial, P.-A. & Billen, M. I. Influence of geometry and eclogitization on oceanic plateau subduction. *Earth Planet. Sci. Lett.* **363**, 34–43 (2013).
14. Stern, R. J., Fouch, M. J. & Klemperer, S. L. An overview of the Izu-Bonin-Mariana subduction factory. in *Geophysical Monograph Series* (ed. Eiler, J.) vol. 138 175–222 (American Geophysical Union, Washington, D. C., 2003).
15. Xu, W., Peng, X., Stern, R. J., Xu, X. & Xu, H. Challenger Deep basalts reveal Indian-type Early Cretaceous oceanic crust subducting in the southernmost Mariana Trench. *Geology* **51**, 865–869 (2023).
16. Zhang, J. *et al.* Mantle serpentinization of subducting plate are controlled by combined effect of plate age and bending curvature. *Earth Planet. Sci. Lett.* **640**, 118799 (2024).

17. Zhang, G., Zhang, J., Wang, S. & Zhao, J. Geochemical and chronological constraints on the mantle plume origin of the Caroline Plateau. *Chem. Geol* **540**, 119566 (2020).
18. Fujioka, K., Okino, K., Kanamatsu, T. & Ohara, Y. Morphology and origin of the Challenger Deep in the Southern Mariana Trench. *Geophys. Res. Lett.* **29**, (2002).
19. Wu, J., Suppe, J., Lu, R. & Kanda, R. Philippine Sea and East Asian plate tectonics since 52 Ma constrained by new subducted slab reconstruction methods. *J. Geophys. Res. Solid Earth* **121**, 4670–4741 (2016).
20. Zhu, G. *et al.* Along-strike variation in slab geometry at the southern Mariana subduction zone revealed by seismicity through ocean bottom seismic experiments. *Geophys. J. Int.* **218**, 2122–2135 (2019).
21. Li, Z., Qiu, X., He, E., Zhang, H. & Wang, Q. Crustal structures of Southmost Mariana Trench revealed by wide-angle seismic profile TS01 (in Chinese with English abstract). *Chin. J. Geophys.* **66**, 4691–4704 (2023).
22. Wan, K. *et al.* Deep Seismic Structure Across the Southernmost Mariana Trench: Implications for Arc Rifting and Plate Hydration. *J. Geophys. Res. Solid Earth* **124**, 4710–4727 (2019).
23. He, E. *et al.* Deep crustal structure across the Challenger Deep: Tectonic deformation and strongly serpentinized layer. *Gondwana Res.* **118**, 135–152 (2023).
24. He, E. *et al.* Strong Serpentinization and Hydration in the Subducting Plate of the Southern Mariana Trench: Insights from Vp/Vs Ratios. *Geophys. Res. Lett.* (2025).
25. Grevemeyer, I., Ranero, C. R. & Ivandic, M. Structure of oceanic crust and serpentinization at subduction trenches. *Geosphere* **14**, 395–418 (2018).
26. Christeson, G. L., Goff, J. A. & Reece, R. S. Synthesis of Oceanic Crustal Structure From Two-Dimensional Seismic Profiles. *Rev. Geophys.* **57**, 504–529 (2019).
27. Christeson, G. L. *et al.* The Yakutat terrane: Dramatic change in crustal thickness across the Transition fault, Alaska. *Geology* **38**, 895–898 (2010).
28. Zhou, Z., Lin, J., Behn, M. D. & Olive, J. Mechanism for normal faulting in the subducting plate at the Mariana Trench. *Geophys. Res. Lett.* **42**, 4309–4317 (2015).
29. Chen, H. *et al.* Deep Outer-Rise Faults in the Southern Mariana Subduction Zone Indicated by a Machine-Learning-Based High-Resolution Earthquake Catalog. *Geophys. Res. Lett.* **49**, e2022GL097779 (2022).
30. Du, M. *et al.* Fluid discharge linked to bending of the incoming plate at the Mariana subduction zone. *Geochem. Persp. Let.* 1–5 (2019) doi:10.7185/geochemlet.1916.
31. Ivandic, M., Grevemeyer, I., Bialas, J. & Petersen, C. J. Serpentinization in the trench-outer rise region offshore of Nicaragua: constraints from seismic refraction and wide-angle data. *Geophys. J. Int.* **180**, 1253–1264 (2010).
32. Contreras-Reyes, E., Grevemeyer, I., Flueh, E. R., Scherwath, M. & Bialas, J. Effect of trench-outer rise bending-related faulting on seismic Poisson's ratio and mantle anisotropy: a case study offshore of Southern Central Chile. *Geophys. J. Int.* **173**, 142–156 (2008).
33. Shillington, D. J. *et al.* Link between plate fabric, hydration and subduction zone seismicity in Alaska. *Nat. Geosci.* **8**, 961–964 (2015).
34. Jokat, W., Altenbernd-Lang, T., Gohl, K., Leitchenkov, G. L. & Eisermann, H. Southernmost Kerguelen Plateau – Not a continental fragment. *Tectonophysics* **910**, 230804 (2025).
35. Contreras-Reyes, E., Grevemeyer, I., Peirce, C. & Obando-Orrego, S. Vp/Vs structure and Pn anisotropy across the Louisville Ridge, seaward of the Tonga-Kermadec Trench. *Tectonophysics* **885**, 230417 (2024).

36. Zhang, J., Zhang, F., Yang, H., Lin, J. & Sun, Z. The effects of plateau subduction on plate bending, stress and intraplate seismicity. *Terra Nova* **34**, 113–122 (2022).
37. Shulgin, A. *et al.* Structural architecture of oceanic plateau subduction offshore Eastern Java and the potential implications for geohazards: Oceanic plateau subduction. *Geophys. J. Int.* **184**, 12–28 (2011).
38. Li, Y. *et al.* Impact of seamounts on the hydration of subducting plates. *Geology* https://doi.org/10.1130/G53355.1 (2025) doi:10.1130/G53355.1.
39. Boneh, Y. *et al.* Intermediate-Depth Earthquakes Controlled by Incoming Plate Hydration Along Bending-Related Faults. *Geophysical Research Letters* **46**, 3688–3697 (2019).
40. Chen, H. *et al.* Along-strike variations in intermediate-depth seismicity in the southernmost Mariana subduction zone: Impact from the subduction of an oceanic plateau. *Tectonophysics* **913**, 230875 (2025).
41. Lin, J., Purdy, G. M., Schouten, H., Sempere, J.-C. & Zervas, C. Evidence from gravity data for focusedmagmatic accretionalong the Mid-Atlantic Ridge. *Nature* **344**, 627–632 (1990).
42. Miura, S. *et al.* Seismological structure and implications of collision between the Ontong Java Plateau and Solomon Island Arc from ocean bottom seismometer–airgun data. *Tectonophysics* **389**, 191–220 (2004).
43. Sleeper, J. D. *et al.* Diffuse spreading, a newly recognized mode of crustal accretion in the southern Mariana Trough backarc basin. *Geosphere* **17**, 1382–1404 (2021).
44. Andikagumi, H., Macpherson, C. G. & McCaffrey, K. J. W. Upper Plate Stress Controls the Distribution of Mariana Arc Volcanoes. *J. Geophys. Res. Solid Earth* **125**, e2019JB017391 (2020).
45. Zang, C., Xu, M., Ni, S. & Wu, W. Improved source parameter estimation of moderate-sized earthquakes in the Southwest Mariana Rift and its implications for arc deformation mechanisms. *Sci. China Earth Sci.* **68**, 2120–2137 (2025).
46. Martinez, F. *et al.* Diffuse Extension of the Southern Mariana Margin. *J. Geophys. Res. Solid Earth* **123**, 892–916 (2018).
47. Scholz, C. H. & Campos, J. On the mechanism of seismic decoupling and back arc spreading at subduction zones. *J. Geophys. Res.* **100**, 22103–22115 (1995).
48. Argus, D. F., Gordon, R. G. & DeMets, C. Geologically current motion of 56 plates relative to the no-net-rotation reference frame: NNR-MORVEL56. *Geochem. Geophys. Geosyst.* **12**, n/a-n/a (2011).
49. Wang, X., Xia, S., Yang, H., Chen, H. & Zhao, D. Structure and dynamics of southern Mariana margin: Constraints from seismicity, tomography and focal mechanisms. *Tectonophysics* **878**, 230300 (2024).
50. Mochizuki, K. *et al.* Recycling of depleted continental mantle by subduction and plumes at the Hikurangi Plateau large igneous province, southwestern Pacific Ocean. *Geology* **47**, 795–798 (2019).
51. Bassett, D. *et al.* Heterogeneous Crustal Structure of the Hikurangi Plateau Revealed by SHIRE Seismic Data: Origin and Implications for Plate Boundary Tectonics. *Geophysical Research Letters* **50**, e2023GL105674 (2023).
52. Bassett, D. *et al.* Crustal Structure of the Hikurangi Subduction Zone Revealed by Four Decades of Onshore-Offshore Seismic Data: Implications for the Dimensions and Slip Behavior of the Seismogenic Zone. *JGR Solid Earth* **130**, e2024JB030268 (2025).
53. Korenaga, J. *et al.* Crustal structure of the southeast Greenland margin from joint refraction and reflection seismic tomography. *J. Geophys. Res.* **105**, 21591–21614 (2000).
54. Zelt, C. A. & Smith, R. B. Seismic traveltime inversion for 2-D crustal velocity structure. *Geophys. J. Int.* **108**, 16–34 (1992).

55. Weissel, J. K. & Anderson, R. N. Is there a Caroline plate? *Earth Planet. Sci. Lett.* **41**, 143–158 (1978).
56. Xu, W., Peng, X., Stern, R. J., Xu, X. & Xu, H. Challenger Deep basalts reveal Indian-type Early Cretaceous oceanic crust subducting in the southernmost Mariana Trench. *Geology* **51**, 865–869 (2023).
57. Zhang, J., Zhang, G. & Wu, J. Geochemical and geochronological constraints on the tectonic and magmatic evolution of the southwestern Mariana subduction zone. *Deep Sea Res. Part I Oceanogr. Res. Pap.* **197**, 104039 (2023).
58. Seton, M. *et al.* A Global Data Set of Present-Day Oceanic Crustal Age and Seafloor Spreading Parameters. *Geochem Geophys Geosyst* **21**, e2020GC009214 (2020).
59. Bird, P. An updated digital model of plate boundaries. *Geochem Geophys Geosyst* **4**, 2001GC000252 (2003).
60. Contreras-Reyes, E. Commentary: Intense Upper Mantle Hydration of the Pacific Plate Beneath the Southern Mariana Trench. *Geophysical Research Letters* **52**, e2025GL116626 (2025).
61. Christensen, N. I. & Mooney, W. D. Seismic velocity structure and composition of the continental crust: A global view. *J. Geophys. Res.* **100**, 9761–9788 (1995).
62. Ekström, G., Nettles, M. & Dziewoński, A. M. The global CMT project 2004–2010: Centroid-moment tensors for 13,017 earthquakes. *Phys. Earth Planet. Inter.* **200–201**, 1–9 (2012).
63. Sandwell, D. T., Müller, R. D., Smith, W. H. F., Garcia, E. & Francis, R. New global marine gravity model from CryoSat-2 and Jason-1 reveals buried tectonic structure. *Science* **346**, 65–67 (2014).
64. Wessel, P. & Smith, W. H. F. New version of the generic mapping tools. *EoS Transactions* **76**, 329–329 (1995).

Acknowledgements

We are grateful to the captain and crew of R/V *Tan Suo Yi Hao*, as well as scientists and technicians who took part in the TS03 cruise. This work was supported by the National Natural Science Foundation of China (42576074, 42476059, 42174110, U25A20791), National Key R&D Program of China (2018YFC0309800), the special fund of South China Sea Institute of Oceanology of CAS (SCSIO2023HC08), State Key Laboratory of Submarine Geoscience (No. sglkfkt2025-10), and Laoshan Laboratory (No. LSKJ202502700). E.H. was supported by the China Scholarship Council (202304910116). The bathymetry data are downloaded from the NCEI and partial multi-beam data were collected onboard R/V *Ke Xue* during the NSFC Open Research Cruise (NORC2023-09) supported by NSFC Shiptime Sharing Project (42249909). We are grateful to Prof. Eduardo Contreras-Reyes for providing codes for calculating plate curvature. We thank Profs. Hongfeng Yang, Gaohua Zhu and Dr. Han Chen for providing high-resolution local earthquake catalogs at the Southern Mariana subduction zone. Dr. Kuiyuan Wan shared velocity model along the profile OBS2016-2. We would also like to thank the Deputy Editor Joe Aslin, the Editorial Board Member Prof. J. Kim Welford and three anonymous reviewers for their insightful comments. Some figures were produced by Generic Mapping Tools (GMT) software[64].

Author contributions

X.Q. and M.X. conceived and directed this research. X.Q., E.H., Y.W. and C.C. participated collection of wide-angle seismic data used in the study. E.H. processed the seismic data and conducted tomographic modelling with the help of I.G. and Y.L. Meanwhile, J.Z. helped in calculation of the plate curvature along different OBS profiles. The interpretation was developed by E.H., X.Q., I.G. and Y.L. in intensive discussion of the results. E.H. and M.Z. designed and drafted the figures. E.Y. and X.Q. wrote the paper, following discussion with, and contributions from, all authors.

Competing interests

The authors declare no competing interests

Editorial summary:

Seismic refraction profiling indicates that subduction initiation of the Caroline Plateau into the Mariana Trench has involved intense faulting and mantle serpentinization at the leading edge of the subducting oceanic plateau

Peer review information:

Communications Earth and Environment thanks the anonymous reviewers for their contribution to the peer review of this work. Primary Handling Editors: J. Kim Welford and Joe Aslin. A peer review file is available.